

Low energy x-ray spectrometer for an electron beam ion trap

P. Beiersdorfer

University of California, Lawrence Livermore National Laboratory, Livermore, California 94550

B. J. Wargelin^{a)}

University of California, Department of Physics and Space Sciences Laboratory, Berkeley, California 94720

(Received 20 August 1993; accepted for publication 18 October 1993)

A flat-crystal spectrometer for analyzing ultrasoft x rays in the wavelength region 10–25 Å was constructed for use on an electron beam ion trap. The spectrometer employs a position-sensitive proportional counter for detection and affords a nominal resolving power of 2000 at a Bragg angle of 45°. Measurements of the *L*-shell spectra of Ne-like Fe¹⁶⁺ and of the $3s_{1/2}$ – $3p_{3/2}$ transitions in near Na-like Pb⁷¹⁺, which fall into the wavelength region from 13.5 to 17.5 Å, are presented demonstrating high throughput and excellent signal-to-noise characteristics. The actual resolving power achieved was limited by the intrinsic resolution of the crystal to 500. A resolving power close to the nominal value was achieved in second order Bragg reflection.

I. INTRODUCTION

The ultrasoft x-ray region between 10 and 25 Å comprises line emission from a wide variety of ions. High-resolution analysis of this region is important for the diagnostics of many types of plasmas ranging from the Sun to tokamaks and laser-produced plasmas as well as for the investigation of basic atomic physics issues. For example, the *K*-shell lines of He-like O, F, Ne, and Na and the *L*-shell lines of Ne-like Fe fall into this wavelength region, which are important diagnostic lines for the Sun and tokamaks; in addition, the wavelength region includes the $n=2$ – 2 and $n=3$ – 3 transitions from very highly charged ions such as the F-like lanthanides and the Na-like noble metals and actinides.

Because of the low energy of the x rays in the ultrasoft x-ray region any spectrometer must be operated *in vacuo* to avoid absorption by air. Although gratings are commonly used to analyze x rays in this region, the photon energy is high enough for employing crystals such as KAP (potassium hydrogen phthalate) or TIAP (thallium hydrogen phthalate) with lattice spacings $2d=25$ – 26 Å. The task of analyzing ultrasoft x rays has been addressed in different ways, each method reflecting the particular characteristics of the source of the x rays. For example, magnetically confined plasmas, such as tokamaks, represent intense extended sources, and the main task of x-ray spectroscopy is the time and space resolved determination of plasma impurities and ion transport.¹ These plasmas have been analyzed with spectrometers employing rapidly rotating flat crystals that provide fast time resolution together with a broad wavelength coverage² or continuous spatial scanning.³ In each case, a set of apertures must be used for collimating the incoming x rays. The photon flux of astrophysical sources, by contrast, is generally small, and efficient light collection over a broad wavelength range takes highest priority. These objectives have been implemented,

for example, in the soft x-ray spectrometer developed for the Advanced X-ray Astrophysics Facility (AXAF).⁴ It employs a curved crystal in the Johann configuration, which greatly improves the light collection efficiency over those of flat-crystal configurations, and uses a gas-filled proportional counter for recording of the dispersed x rays with high quantum efficiency.

Like astrophysical sources, the electron beam ion trap (EBIT) is a relatively weak x-ray source, and the efficient recording of high-resolution spectra that enable accurate wavelength determinations represents the main objective of x-ray spectroscopy. The EBIT source uses a compressed electron beam with a precisely controlled energy to produce and excite stationary, electrostatically trapped ions of any preselected charge state, in principle up to bare uranium.⁵ Because x rays are emitted only from the region where the electron beam interacts with the ions, the EBIT source is cylindrical with a 2-cm length and 60- μ m width, as given by the length of the trap and the diameter of the electron beam. The source dimensions are thus similar to those of an entrance slit for a grating spectrometer and are well matched for either flat-crystal or von Hámos-type bent-crystal spectrometers. A spectrometer of the latter type is already in use on EBIT to analyze x rays with energies above about 2 keV.⁶ It operates in a helium atmosphere, which is separated from EBIT by a 5-mil (125- μ m) beryllium window. Because alignment of a von Hámos-type spectrometer is difficult to accomplish *in vacuo*, we opted to develop an easy-to-align flat-crystal spectrometer for analyzing x rays in the ultrasoft x-ray region with energies below 2 keV. To compensate for the lower efficiency of the flat-crystal geometry compared to that of a comparably sized von Hámos geometry, we have developed a position-sensitive detector with a nearly 100% quantum efficiency for low-energy x rays that can be deployed *in vacuo*.

We illustrate the performance of the low-energy crystal spectrometer by presenting measurements of the *L*-shell spectrum of Ne-like Fe. We also have made a measurement of the $3s_{1/2}$ – $3p_{3/2}$ transition energies in Na-like, Mg-like,

^{a)}Present address: Harvard-Smithsonian Center for Astrophysics, 60 Garden St., Cambridge, MA 02138.

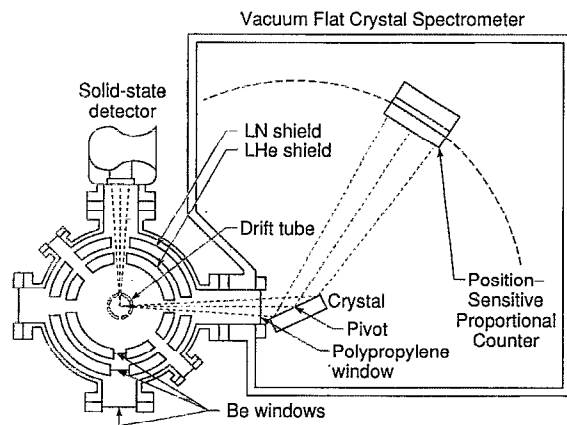


FIG. 1. Schematic layout of the flat-crystal spectrometer on the EBIT facility. The electron beam direction is out of the page and represents a line source 2 cm long and 60 μm in diameter so that no entrance slit is needed. Crystal and detector rotate about a common pivot point. The vacuum of the spectrometer is separated from the EBIT vacuum by a thin foil consisting of either 4 μm polypropylene or 1 μm polyimide.

Al-like, and Si-like Pb. The latter measurement allows us to compare the performance of our new instrument with a Johann-type crystal spectrometer with a microchannel plate detector and two-dimensional readout⁷ used earlier on EBIT to measure the $3s_{1/2}$ - $3p_{3/2}$ transition energy of Na-like Pt. We find that the new flat-crystal spectrometer has a higher efficiency with comparable resolving power.

II. DESCRIPTION OF INSTRUMENT

Figure 1 shows a schematic of the flat-crystal spectrometer we designed for use in the ultrasoft x-ray region. The diffraction plane is oriented perpendicular to the electron beam. The spectrometer employs a $2 \times 5\text{-cm}^2$ analyzing crystal. The crystal and detector rotate around a common pivot point, allowing for easy alignment. The maximum attainable Bragg angle is 63°.

The instrument employs a 10-cm long, one-dimensional position-sensitive proportional counter with P-10 fill gas (90% Ar, 10% CH₄) at 1 atm flowing through the chamber at a steady rate of 10–20 mm³/s. The $0.8 \times 8.0\text{-cm}^2$ detector window consists of a 4- μm thick polypropylene foil coated with a few hundred Å (<200) of aluminum. It is supported down the middle by one 1-mm wide horizontal bar. Independent pressure tests show that the thin window can withstand pressures exceeding 4 or 5 atm. Fatigue caused by cycling the vacuum, however, may cause microscopic perforations in the window indicated by poorer vacuum performance, which necessitate a periodic replacement of the window. The same type of foil is used to separate the spectrometer vacuum (8×10^{-7} Torr) from the much higher vacuum of the EBIT vessel ($\sim 10^{-10}$ Torr). Without this separation the vacuum in the EBIT trap (typically $\sim 10^{-12}$ Torr) degrades significantly, depressing the attainable charge balance by charge-exchange recombination with neutral background gases. The foil has a diameter of 25 mm. Unlike the foil covering the detector window, this foil is free-standing and cannot withstand a pressure differential of an atmosphere. As a result, we use

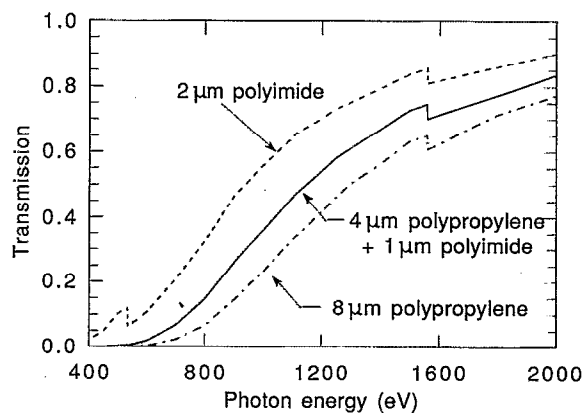


FIG. 2. Approximate x-ray transmission curves for three combinations of two foils consisting of 4 μm polypropylene or 1 μm polyimide coated with 200 Å of aluminum.

a by-pass pumpline during the evacuation of the spectrometer to maintain nearly equal pressure on both sides of the foil.

Absorption of low-energy x rays in the two Al-coated polypropylene foils limits the useful range of the spectrometer, i.e., the range where the transmission is larger than 5%, to wavelengths less than about 16 Å, as shown in Fig. 2. We have also operated the spectrometer by replacing one of the 4- μm polypropylene foils by a 1- μm polyimide foil. Polyimide foils have been successfully used in the low-energy crystal spectrometer constructed for AXAF.⁸ This extends the useful range of the spectrometer to about 19 Å. Substituting polyimide for both polypropylene foils extends the useful range of the spectrometer to wavelengths longer than can be analyzed by hydrogen phthalate crystals, i.e., to wavelengths longer than 25 Å.

The combined distance between EBIT, crystal, and detector is 50 cm. The detector resolution is about 250 μm and thus provides an angular resolution of $\Delta\theta = 5 \times 10^{-4}$. Using Bragg's law

$$n\lambda = 2d \sin \theta,$$

where d is the lattice spacing of the crystal and n is the order of reflection of a line with wavelength λ at an angle θ , the nominal resolving power of the spectrometer is given by

$$\lambda/\Delta\lambda = \tan \theta/\Delta\theta.$$

As a result, the nominal resolving power of our instrument is as high as $\lambda/\Delta\lambda = 2000$ at a Bragg angle of $\theta = 45^\circ$. For the measurements presented below we used TIAP or CsAP crystals (with $2d$ spacings of 25.76 and 25.68 Å, respectively⁹). Their intrinsic resolving power in first order Bragg reflection limited the measurements to $\lambda/\Delta\lambda = 500$ –900; a resolving power near the nominal value was achieved, however, in second order Bragg reflection.

III. PERFORMANCE AND SPECTRAL MEASUREMENTS

A composite spectrum of the $2p$ - $3s$ and $2p$ - $3d$ transitions of Ne-like Fe¹⁶⁺ is shown in Fig. 3. Three settings of the spectrometer were used to record the data shown; the

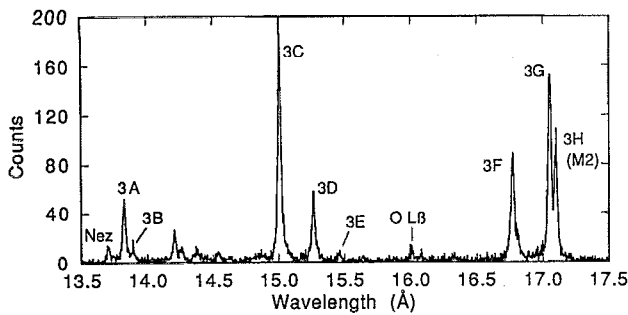


FIG. 3. Spectrum of the *L*-shell lines in neonlike Fe XVII recorded at an electron beam energy of 1300 V and a beam current of 45 mA. The spectrum is a composite of data from three spectrometer settings each recording for 75 min. The Fe XVII lines are labeled in the notation of Table I. Unlabeled lines are from Fe XVIII.

three individual spectra were joined at 14.8 and 16.3 Å to form the composite shown in Fig. 3. The observations were made by setting the beam energy to 1.3 keV, i.e., to a value just above the 1260-eV ionization threshold of Ne-like Fe. The accumulation time for each spectrum is about 75 min. The Ne-like Fe lines are labeled in the notation of Parkinson.¹⁰ Unlabeled lines (between 14.0 and 14.5 Å) are from F-like Fe. In addition, two features from indigenous impurities in EBIT can be identified: the Lyman-β line of H-like O, labeled O *L*β, and the forbidden line in He-like Ne from the $1s2s\ ^3S_1$ upper level, labeled Ne *z*.

A summary of the wavelengths measured for each Ne-like Fe transition is given in Table I. The wavelengths of the iron lines are determined relative to hydrogenic or He-like reference lines, which are measured before or after recording the Fe spectra. In particular, the region with the Ne-like Fe $2p-3s$ lines is calibrated by the *K*α emission from He-like F. Here we use the $1s2p\ ^1P_1$ resonance and $1s2s\ ^3S_1$ forbidden line as reference lines and set their wavelengths to the values calculated by Drake,¹¹ 16.8064 and 17.1528 Å, respectively. The region containing the $2p-3d$ lines is calibrated by the Ly-γ, Ly-δ, Ly-ε, and Ly-η lines of H-like oxygen (cf. Fig. 4), the wavelengths of which we set to 15.1762, 14.8206, 14.6343, and 14.5243 Å, as calculated by Garcia and Mack.¹² The *K*β and *K*γ transitions in He-like F are used as reference lines to calibrate the region

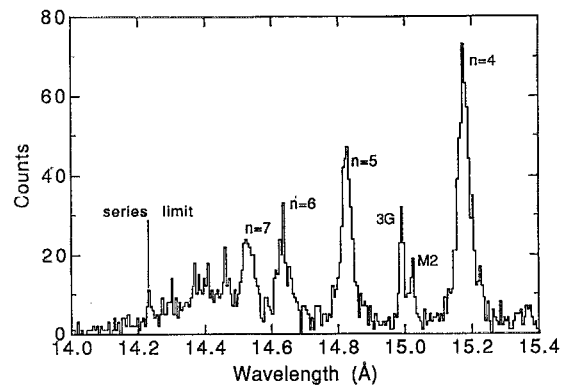


FIG. 4. Spectrum of the Lyman series of hydrogenic O VIII. The spectrum was recorded during a 45-min interval with the electron beam energy and current set to 3.7 kV and 193 mA, respectively. Two $2p-3s$ transitions in neonlike Kr XXVII, labeled 3G and M2, are seen near 15 Å. These lines are observed in second order Bragg reflection. Note their much narrower line widths.

with the $2s-3p$ Fe transitions. Their wavelengths are set to 14.4588 and 13.7819 Å, as calculated by Vainshtein and Safronova.¹³ A comparison of our iron lines with those measured in solar observation^{10,14,15} shows reasonable agreement considering the amount of scatter among the results from the solar measurements.

The observed line width is commensurate with that expected from the rocking curve of the crystal, and is about $\lambda/\Delta\lambda=400-500$ for the Fe lines. In second order Bragg reflection the resolving power of the crystal is greatly improved, reaching values of 3000–4000, and so the widths of lines measured in second order should be much narrower. This is indeed observed. Inspection of Fig. 4 reveals two very sharp lines between the Ly-γ and Ly-δ lines of H-like oxygen. Their widths correspond to $\lambda/\Delta\lambda=1000$, which is closer to the nominal resolving power of 1400 that we expect from the angular resolution of the detector a Bragg angle of 35° and close to the value of 1200 obtained if we account for the intrinsic crystal resolution in quadrature. The lines are identified as the $2p-3s$ electric dipole transition 3G and the $2p-3s$ magnetic quadrupole transition M2 in Ne-like Kr (cf. Table I). Krypton is an indigenous back-

TABLE I. Summary of measured wavelengths of *L*-shell transitions in neonlike Fe (in Å). Values in parentheses indicate the uncertainty in the last digit. Values from previous measurements are given for comparison. All transitions are to the $(2s^22p^6)_{J=0}$ ground state.

Key	Upper level	λ^a	λ^b	λ^c	λ^d
3A	$(2s_{1/2}2p^53p_{3/2})_{J=1}$	13.825(1)	13.824	13.847	13.824
3B	$(2s_{1/2}2p^53p_{1/2})_{J=1}$	13.889(2)	13.888		13.890
3C	$(2s^22p_{1/2}^53d_{3/2})_{J=1}$	15.009(1)	15.013	15.013	15.012
3D	$(2s^22p_{3/2}^53d_{5/2})_{J=1}$	15.265(2)	15.259	15.262	15.255
3E	$(2s^22p_{3/2}^53d_{3/2})_{J=1}$	15.456(4)	15.449	15.456	15.451
3F	$(2s^22p_{1/2}^53s_{1/2})_{J=1}$	16.772(3)	16.769	16.775	16.775
3G	$(2s^22p_{3/2}^53s_{1/2})_{J=1}$	17.054(1)	17.041	17.043	17.051
3H(M2)	$(2s^22p_{3/2}^53s_{1/2})_{J=2}$	17.099(1)	17.086	17.084	17.096

^aPresent measurements.

^bReference 10.

^cReference 14.

^dReference 15.

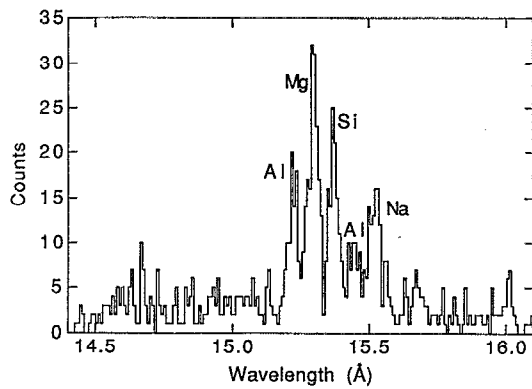


FIG. 5. Spectrum of the $3s_{1/2}$ - $3p_{3/2}$ transitions in sodiumlike, magnesiumlike, aluminumlike, and siliconlike lead, Pb LXIX-LXXII. The spectrum was recorded during a 57-min interval with the beam energy and current set to 29 kV and 140 mA, respectively.

ground impurity in EBIT, and observation of these lines comes as no surprise.

The intrinsic energy resolution of the proportional counter given by the x-ray pulse height distribution is sufficient to discriminate between pulses in first and second order. We use this capability routinely to effectively eliminate lines from one of the orders.

Finally, we present a spectrum of the $3s_{1/2}$ - $3p_{3/2}$ transitions in Na-like Pb and in ions of neighboring charge states shown in Fig. 5, as this allows us to compare the performance of our flat-crystal spectrometer to that of a bent-crystal spectrometer of the Johann type used on EBIT to measure the $3s_{1/2}$ - $3p_{3/2}$ transition in Na-like Pt.⁷ Measurements of this transition provides a sensitive test of relativity and quantum electrodynamics, and highly efficient spectrometers are needed to provide reliable data for many ions along the isoelectronic sequence for systematic comparisons with theory. The Johann-type crystal spectrometer on EBIT employed a cylindrically bent RAP crystal with a 58-cm radius of curvature and a two-dimensional microchannel plate detector with wedge and strip readout. The instrument was directly connected to EBIT without windows separating the vacua in the spectrometer and EBIT. The EBIT line source was located on the Rowland circle and oriented perpendicular to the diffraction plane. Because of the narrowness of the source the instrument needed to be rocked back and forth to scan over a range of Bragg angles, and the acquisition of a single spectrum required about 2 h.⁷

By contrast, the spectrum of Na-like Pb recorded with the new flat-crystal spectrometer shown in Fig. 6 required a 57-min observation time and covers a broad range of Bragg angles that includes not only the Na-like transition but also transitions in the neighboring Mg-like, Al-like, and Si-like charge states. The efficiency of the flat-crystal spectrometer ions is highly competitive with the Johann-type instrument. In addition, the new instrument records a wider spectral range and exceeds the Johann-type instrument in the ease of the alignment and operation.

An overview of the $3s_{1/2}$ - $3p_{3/2}$ transitions is given in Table II. These transitions fall into the wavelength region subtended by the H-like O transitions shown in Fig. 4, and we used the H-like O transitions for calibration. The measured wavelengths are listed in Table II, and we find 15.519 ± 0.005 Å, or 798.92 ± 0.25 eV, for the $3s_{1/2}$ - $3p_{3/2}$ transition in Na-like Pb. Wavelengths computed with a multiconfiguration Dirac-Fock calculation in the extended average-level approach^{16,17} are also listed in Table II for comparison. The precision of our measurement is limited by the small number of counts in each peak. Observation times longer than the 57-min interval of the present measurement will improve the precision considerably in future measurements. Nevertheless, our measurement is already comparable in accuracy to a much more elaborate measurement of 3-3 transition in Na-like Pb performed on the Unilac accelerator facility and reported very recently.¹⁸ The Unilac measurement reported 798.65 ± 0.13 eV for a blend of the Na-like $3s$ - $3p$ transition and several Ne-like transitions, which is in agreement with our value.

IV. DISCUSSION

We have described an efficient flat-crystal spectrometer for use on an electron beam ion trap and presented several representative measurements in the wavelength region above 13 Å (i.e., energies less than 1 keV). At present, the accuracy of our wavelength determinations is limited by the intrinsic resolving power of the TIAP and CsAP crystals used. Better precision may be achieved in the future by using a KAP or mica crystal. In addition to the measurements in the ultrasoft x-ray regime, the spectrometer represents a convenient tool for measuring transitions at x-ray energies above 1 keV, as indicated by the measurements of the L -shell transitions in Ne-like Kr with energies near 1.6 keV. To maintain a near 100% quantum efficiency for higher energy x-rays the detector was tested and successfully operated with a full gas consisting of 90% Kr and

TABLE II. Summary of measured wavelengths of $3s_{1/2}$ - $3p_{3/2}$ transitions in sodiumlike through siliconlike Pb. Values in parentheses indicate the uncertainty in the last digit. Theoretical wavelengths are from multiconfiguration Dirac-Fock (MCDF) calculations (Ref. 17).

Key	Ion	Transition	$\lambda_{\text{measured}}$ (Å)	λ_{MCDF} (Å)
Si	Pb ⁶⁸⁺	$(3s_{1/2}3p_{1/2}^23p_{3/2})_{J=1} \rightarrow (3s^23p^2)_{J=0}$	15.366(3)	15.365
Al-1	Pb ⁶⁹⁺	$(3s_{1/2}3p_{1/2}2p_{3/2})_{J=3/2} \rightarrow (3s^23p_{1/2})_{J=1/2}$	15.437(6)	15.433
Al-2	Pb ⁶⁹⁺	$(3s_{1/2}3p_{1/2}2p_{3/2})_{J=1/2} \rightarrow (3s^23p_{1/2})_{J=1/2}$	15.217(4)	15.182
Mg	Pb ⁷⁰⁺	$(3s_{1/2}3p_{3/2})_{J=1} \rightarrow (3s^2)_{J=0}$	15.292(2)	15.267
Na	Pb ⁷¹⁺	$3p_{3/2} \rightarrow 3s_{1/2}$	15.519(5)	15.509

10% CH₄. Operating the spectrometer in this mode allows us to completely complement the spectra recorded with the EBIT von Hámos-type spectrometer.

ACKNOWLEDGMENTS

We are grateful to M. H. Chen and A. L. Osterheld for their calculations of the $3s-3p$ transition energies and line intensities, and we thank A. Ya. Faenov and T. H. Markert for providing the CsAP crystal and the polyimide foils. This spectrometer was constructed under NASA Grant No. NAGW-2688. The work was performed at Lawrence Livermore National Laboratory under the auspices of the Department of Energy under Contract No. W-7405-ENG-48.

¹U. Schumacher, R. Barnsley, G. Fussmann, K. Assmussen, C. C. Chu, and G. Janeschitz, *AIP Conf. Proc.* **257**, 131 (1992).

²R. Barnsley, K. D. Evans, N. J. Peacock, and N. C. Hawkes, *Rev. Sci. Instrum.* **57**, 2159 (1986).

³U. Schumacher, E. Källne, H. W. Morsi, and G. Rupprecht, *Rev. Sci. Instrum.* **60**, 562 (1989).

⁴T. H. Markert, T. R. Powers, A. M. Levine, C. B. McCullum, J. J. Mohr, and C. R. Canizares, *Proc. SPIE* **982**, 245 (1988).

⁵M. A. Levine, R. E. Marrs, J. R. Henderson, D. A. Knapp, and M. B. Schneider, *Phys. Scr.* **T22**, 157 (1988); R. E. Marrs, M. A. Levine, D. A. Knapp, and J. R. Henderson, *Phys. Rev. Lett.* **60**, 1715 (1988).

⁶P. Beiersdorfer, R. E. Marrs, J. R. Henderson, D. A. Knapp, M. A. Levine, D. B. Platt, M. B. Schneider, D. A. Vogel, and K. L. Wong, *Rev. Sci. Instrum.* **61**, 2338 (1990).

⁷T. E. Cowan *et al.*, *Phys. Rev. Lett.* **66**, 1150 (1991).

⁸T. H. Markert *et al.*, *Proc. SPIE* **1549**, 408 (1991).

⁹A. Burek, *Space Sci. Instrum.* **2**, 53 (1976).

¹⁰J. H. Parkinson, *Astron. Astrophys.* **24**, 215 (1973).

¹¹G. W. F. Drake, *Can. J. Phys.* **66**, 586 (1988).

¹²J. D. Garcia and J. E. Mack, *J. Opt. Soc. Am.* **55**, 654 (1965).

¹³L. A. Vainshtein and U. I. Safronova, *Phys. Scr.* **31**, 519 (1985).

¹⁴D. L. McKenzie, P. B. Landecker, R. M. Broussard, H. R. Rugge, R. M. Young, U. Feldman, and G. A. Doschek, *Astrophys. J.* **241**, 409 (1980).

¹⁵K. J. H. Phillips *et al.*, *Astrophys. J.* **256**, 774 (1982).

¹⁶I. P. Grant, B. J. McKenzie, P. H. Norrington, D. F. Mayers, and N. C. Pyper, *Comput. Phys. Commun.* **21**, 207 (1980).

¹⁷M. H. Chen (private communication, 1993).

¹⁸A. Simionovici, D. D. Dietrich, R. Keville, T. Cowan, P. Beiersdorfer, M. H. Chen, and S. A. Blundell, *Phys. Rev. A* **48**, 3056 (1993).